Electronic Supplementary Information

In-situ transformation of bismuth metal-organic frameworks for efficiently selective electroreduction of CO_2 to formate

Wei-Wen Yuan [a], Jian-Xiang Wu [a], Xiang-Da Zhang [a], Shu-Zhen Hou [a], Ming Xu [a] and Zhi-Yuan Gu [a*]

[a]Jiangsu Key Laboratory of Biofunctional Materials, Jiangsu Collaborative Innovation Center of Biomedical Functional Materials, Jiangsu Key Laboratory of New Power Batteries, College of Chemistry and Materials Science, Nanjing Normal University, Nanjing 210023, China

*Corresponding author: Prof. Zhi-Yuan Gu, Email: guzhiyuan@njnu.edu.cn.

Calculation details [1-3]

Potential conversion (E)

All potentials were converted to the reversible hydrogen electrode (RHE) reference scale following the equation:

$$E\ (vs.\ RHE) = E\ (vs.\ Ag/AgCl) + 0.19\ V + 0.0591\ V \times pH.$$

Faradaic efficiency (FE)

$$FE_{gas} = \frac{Q_{gas}}{Q_{total}} \times 100\% = \frac{V_a \times (10\ mL/min) \times N \times F \times 1\ cm^{-2}}{(60\ s/min) \times (24000\ cm^3/mol) \times J} \times 100\%$$

Where V_a is the volume concentration of H_2 or CO calculated by a calibration of the gas chromatography (GC), N=2 is the number of transferred electrons for certain product, F is the Faraday constant (96485 C mol^{-1}), and J is the recorded current density (mA cm^{-2}).

$$FE_{HCOO^-} = \frac{Q_{HCOO^-}}{Q_{total}} \times 100\% = \frac{n_{HCOO^-} \times N \times F}{t \times J} \times 100\%$$

Where n_{HCOO^-} is the amount of formate calculated by a calibration of the high-performance liquid chromatography (HPLC) and t is the electrochemical reaction time.

Electrochemically active surface areas (ECSA)

$$ECSA = R_f \times S = \frac{C_{dl}}{21\ \mu F/cm^2} \times S = \frac{\Delta J}{v \times 21\ \mu F/cm^2} \times S$$

S is the geometric area of the working electrode (in this work, S=1.0 cm^{-2}). R_f is the roughness factor, which is obtained by double-layer capacitance C_{dl} for the working electrode and the corresponding working electrode (in this work, the average double-layer capacitance is 21 μF cm^{-2} [4]). C_{dl} is estimated by plotting the $\Delta J = (J_a - J_c)$ at 0.587 V vs. RHE, where J_a and J_c was respective the anodic and cathodic current density from cyclic voltammetry (CV) measurement in N_2-saturated 0.5 M $KHCO_3$ electrolyte against v, which is the scan rate (mV s^{-1}). The value of slope is twice that of C_{dl}. Moreover, the potentials of CVs are from 0.582 to 0.592 V vs. RHE and scan rates are from 20 to 100 mV s^{-1}.

Turnover Frequency (TOF)

$$TOF = \frac{J_{total} \times FE_{HCOO^-}}{N} \times \frac{v}{Area} \times 3600\ s/h$$

Where J_{total} is the total current density, N=2 is the number of transferred electrons for formate, v= 10 mV s^{-1}, and the area is reckoned by cathodic curve in N_2-saturated situation.

Tafel slope

Tafel slopes for formate production are calculated from the geometric current densities and the formate Faradaic efficiency (overpotentials versus logJ_{HCOO^-}).

Figures and tables

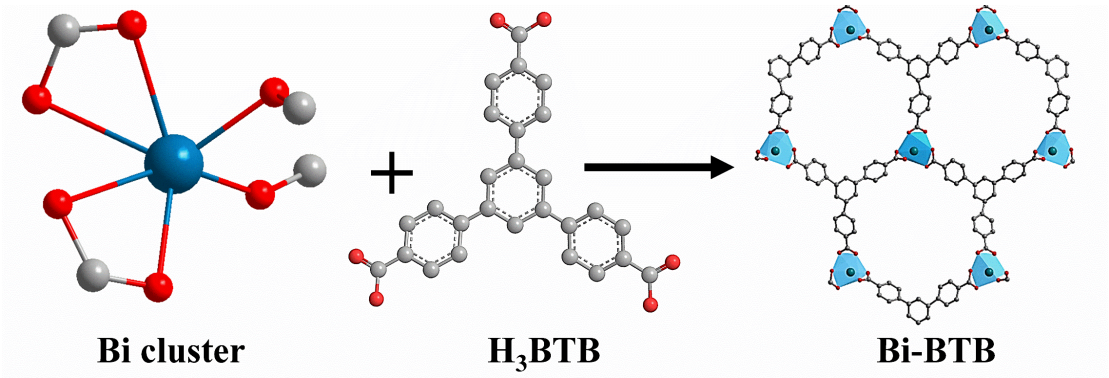

Fig. S1 Synthetic route of Bi-BTB. Red is O, grey is C and purplish blue is Bi.

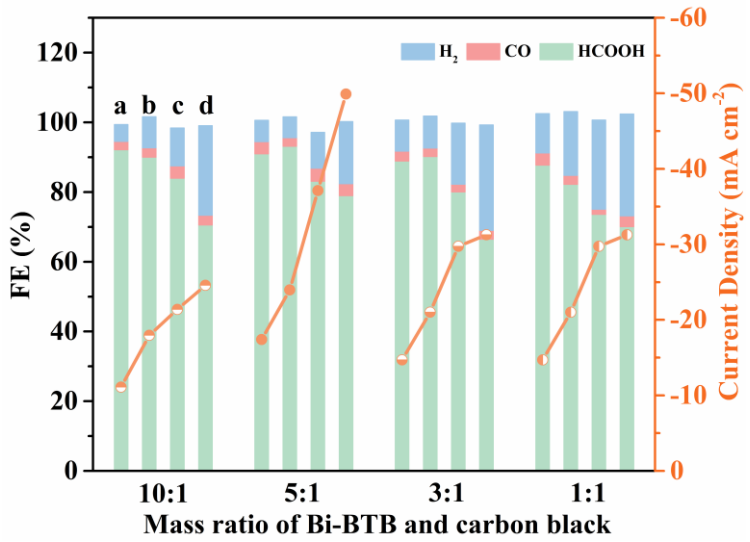

Fig. S2 Faradaic efficiencies and total current densities over different mass ratio of Bi-BTB to carbon black at different potentials. (a, b, c and d represent the potentials at -0.719 V, -0.819 V, -0.919 V and -1.019 V vs. RHE, respectively) For the preparation of working electrodes, 1 mg Bi-BTB on each carbon paper is fixed for the quantitative optimization, meanwhile, the mass of carbon black is the variable. For example, the mass ratios for 10:1 and 5:1 represent that 1 mg Bi-BTB with 0.1 mg of carbon black and 1 mg Bi-BTB with 0.2 mg of carbon black, respectively.

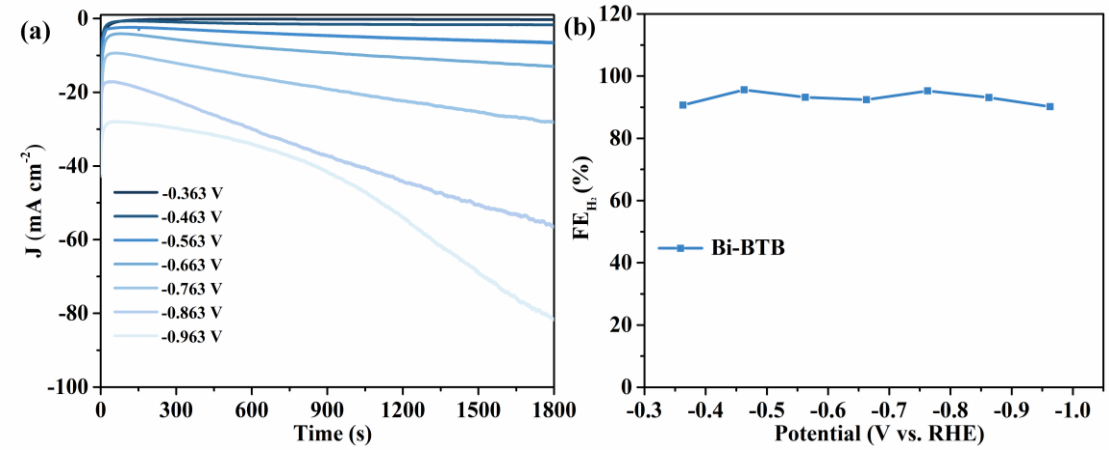

Fig. S3 (a) Total current density of Bi-BTB in N_2-saturated 0.5 M $KHCO_3$ electrolyte at different potentials from -0.363 V to -0.963 V vs. RHE as indicated. (b) Faradaic efficiencies of H_2 for Bi-BTB at each applied potential.

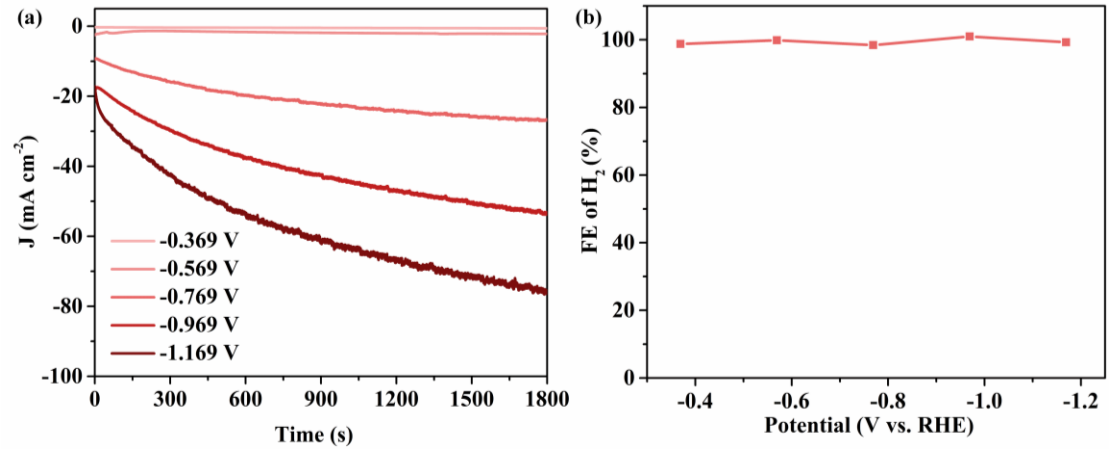

Fig. S4 (a) Total current density of H_3BTB in CO_2-saturated 0.5 M $KHCO_3$ electrolyte at different potentials from -0.369 V to -1.169 V vs. RHE as indicated. (b) Faradaic efficiencies of H_2 for H_3BTB at each applied potential.

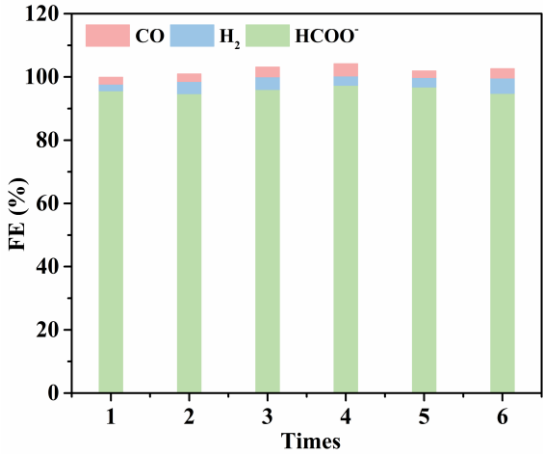

Fig. S5 Faradaic efficiencies at -0.669 V vs. RHE using the same Bi-BTB electrode for six times.

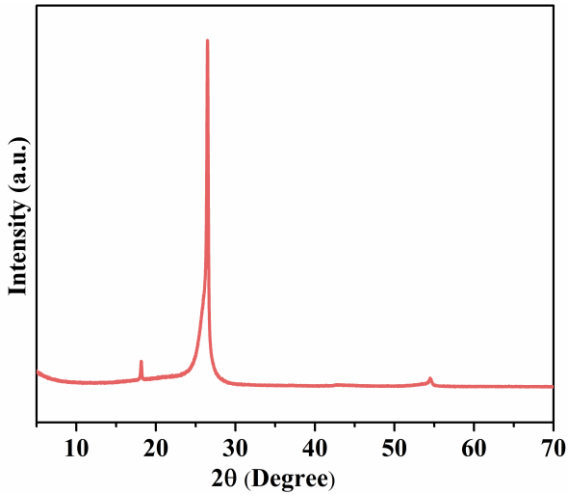

Fig. S6 XRD pattern of carbon black dispersed on carbon paper.

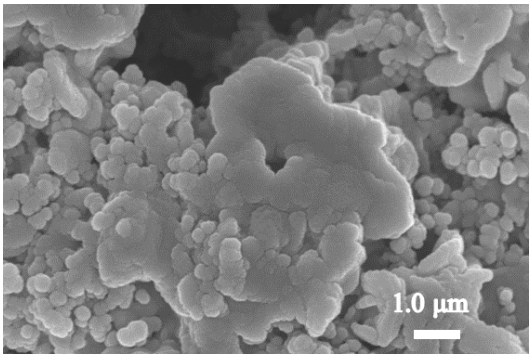

Fig. S7 SEM image of Bi-BTB mixed with carbon black dropped on carbon paper after eCO_2RR 1 h in CO_2-saturated 0.5 M $KHCO_3$ electrolyte.

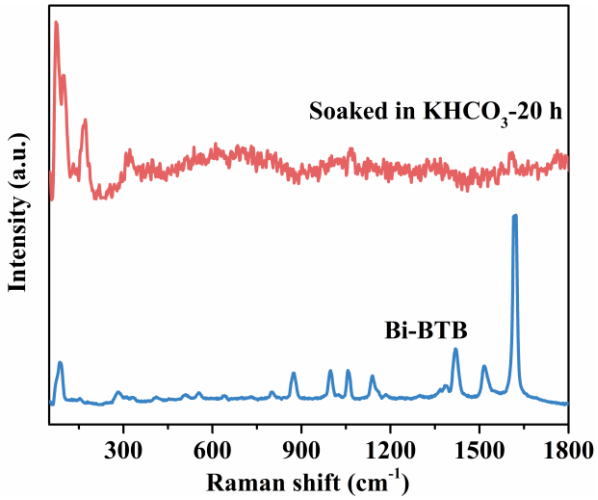

Fig. S8 Raman scattering spectra of pristine Bi-BTB (blue) and Bi-BTB soaked in $KHCO_3$ after 20 h (red). The Raman characteristic bands at around 78, 102 and 168 cm^{-1}, which are related to vibrational modes of Bi=O bond lattice, while the band at 1074 cm^{-1} is assigned to symmetric stretching of CO_3^{2-}.

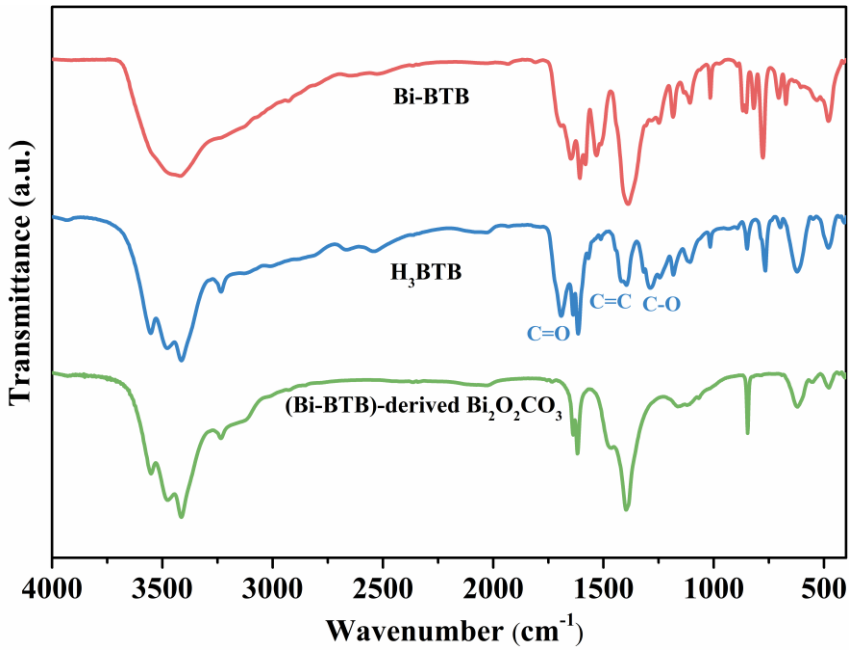

Fig. S9 FT-IR spectrum of H_3BTB, Bi-BTB, and (Bi-BTB)-derived $Bi_2O_2CO_3$. For the pure ligand H_3BTB, the strong absorption at 1695 cm^{-1} is from the carboxylic acid C=O stretching vibrations. The aromatic C=C bond appears at 1421 cm^{-1}, while the C-O bond in carboxylic acid group appears at 1288 cm^{-1}. Compared with Bi-BTB and H_3BTB, there is no carboxylic acid C=O characteristic peak of (Bi-BTB)-derived $Bi_2O_2CO_3$, which can prove H_3BTB ligands have been completely replaced by HCO_3^-.

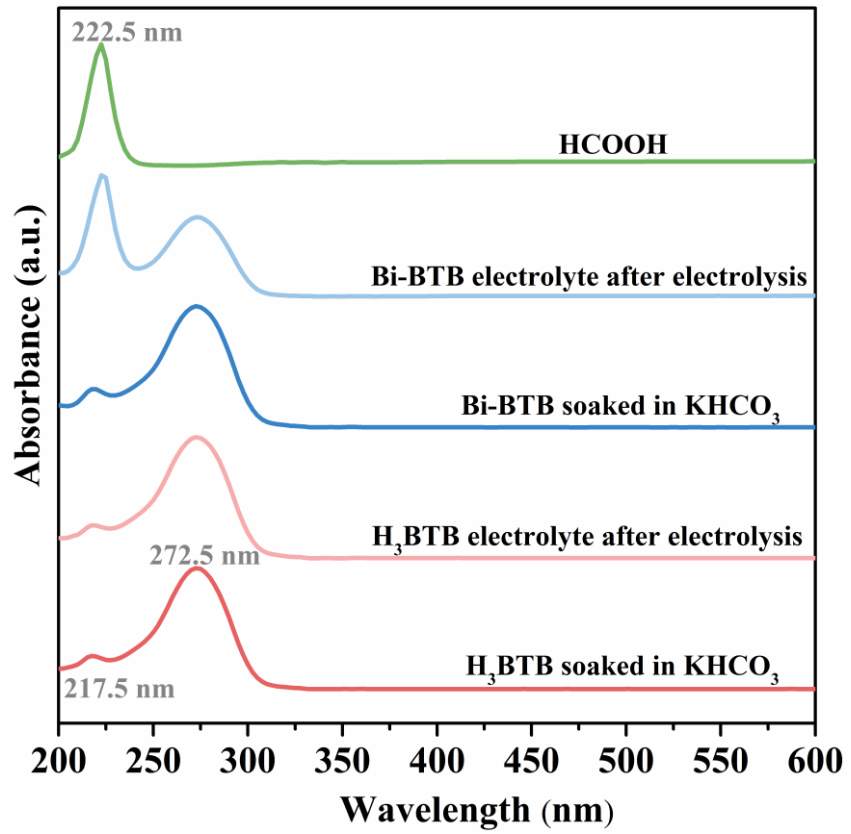

Fig. S10 UV-vis spectra of HCOOH (green), the electrolyte of Bi-BTB/carbon paper electrode (skyblue) and H_3BTB/carbon paper electrode (salmon) after electrolysis for 0.5 h, and the solution of Bi-BTB (darkblue) and H_3BTB (firebrick) after soaking in electrolysis. It is noted that the experimental data are obtained under the background of deducting 0.5 M $KHCO_3$. The characteristic absorbance peaks centered at 217.5 and 272.5 nm belong to H_3BTB. Moreover, the peak centered at 222.5 nm attributes to HCOOH. The results show that H_3BTB is replaced by HCO_3^- and then exists in electrolyte during the in-situ MOFs transformation process.

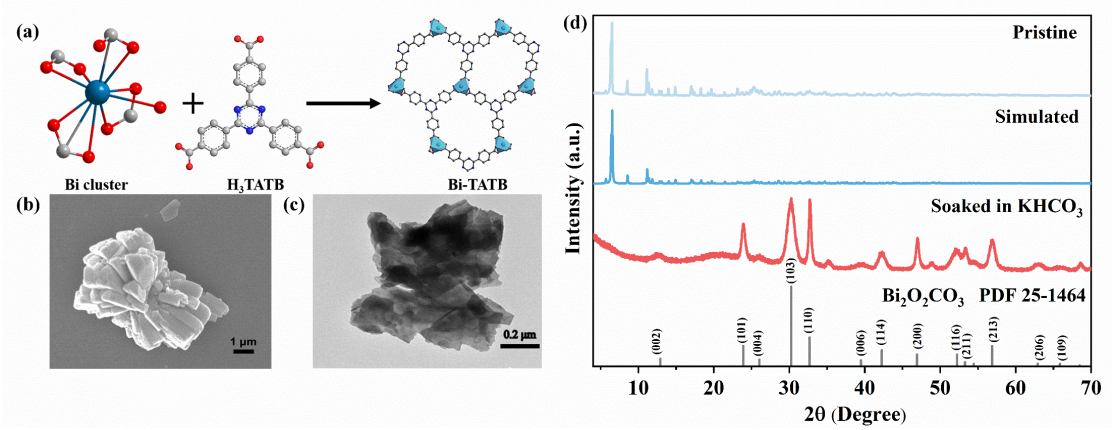

Fig. S11 (a) Synthetic route of Bi-TATB. (b) SEM image and (c) TEM image of pristine Bi-TATB. (d) XRD patterns of pristine Bi-TATB (skyblue) and Bi-TATB after soaking in 0.5 M $KHCO_3$ electrolyte for 20 h (red). Red is O, grey is C, blue is N, and purplish blue is Bi.

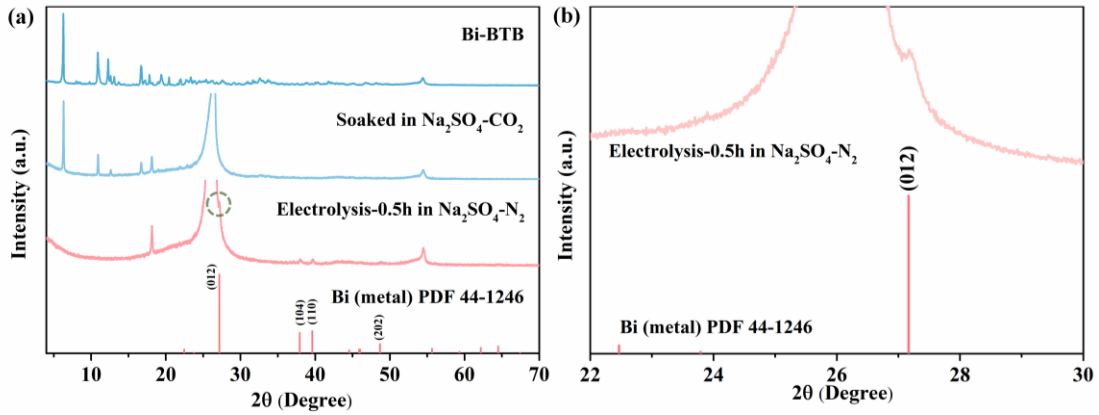

Fig. S12 (a) XRD patterns of Bi-BTB for research on the stability after applying a reducing potential at -0.869 V vs. RHE in CO_2- and N_2-saturated 0.25 M Na_2SO_4 electrolyte; (b) The magnification of the region marked by a green dotted circle in figure (a).

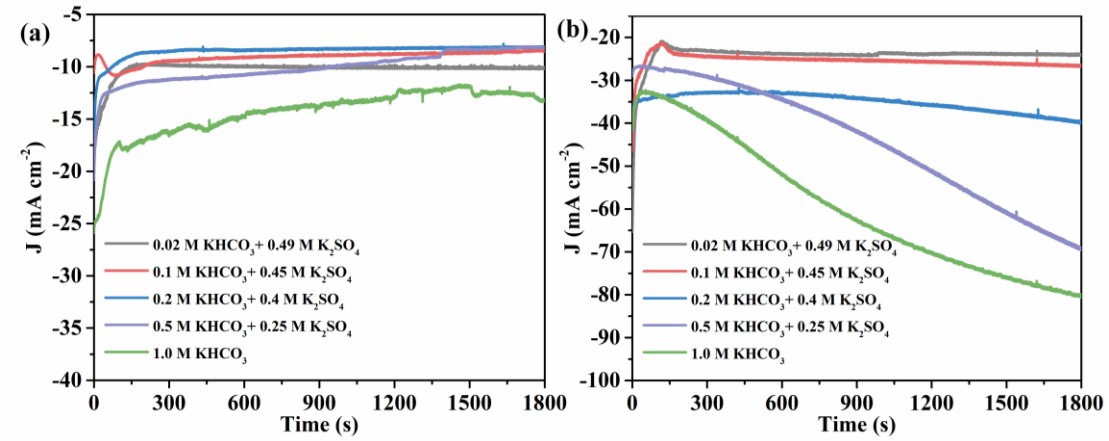

Fig. S13 Total current density of formate versus different potassium bicarbonate concentrations at the potentials of (a) -0.669 V and (b) -1.069 V vs. RHE, respectively.

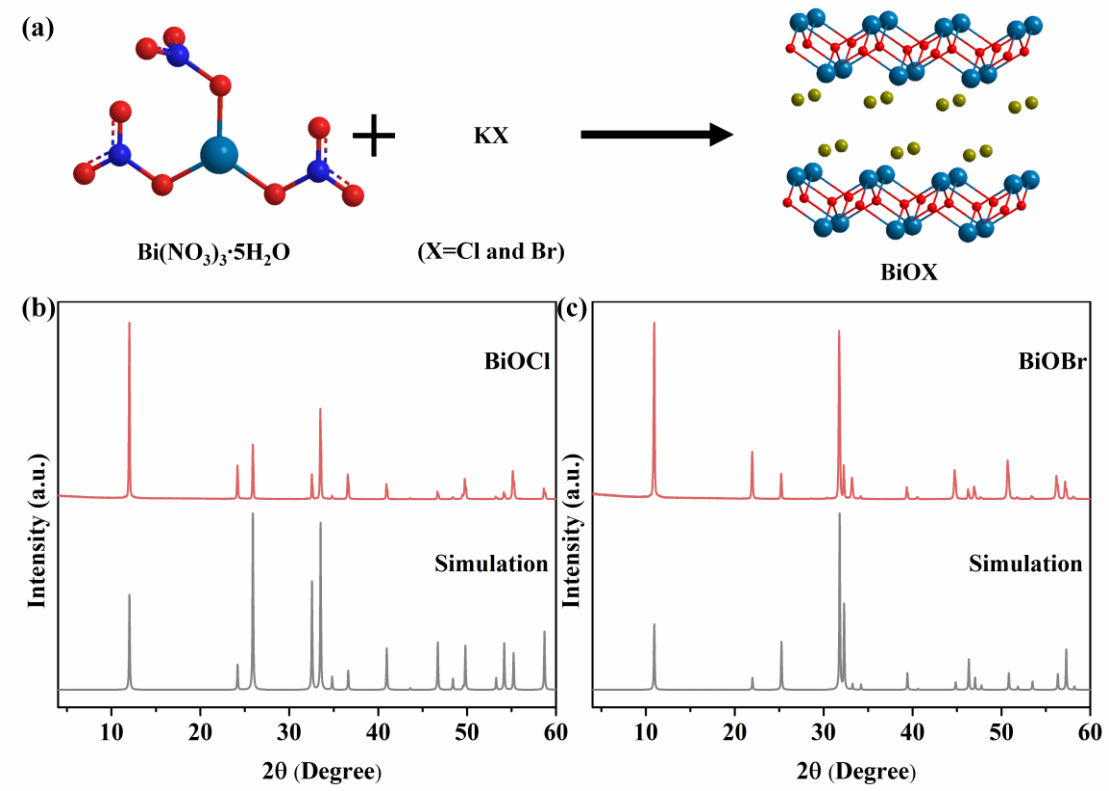

Fig. S14 Synthetic route (a), XRD patterns of (b) BiOCl and (c) BiOBr. Red is O, grey is K, blue is N, olive is X (X= Cl and Cl Br) and purplish blue is Bi.

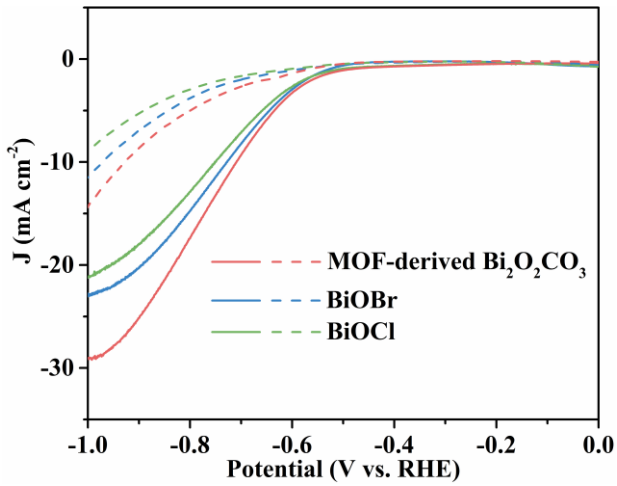

Fig. S15 Measured LSV curves of MOF-derived $Bi_2O_2CO_3$, BiOCl and BiOBr at 10 mV s^{-1}. The dotted and solid line separately reacted in N_2- and CO_2-saturated 0.5 M $KHCO_3$ electrolyte.

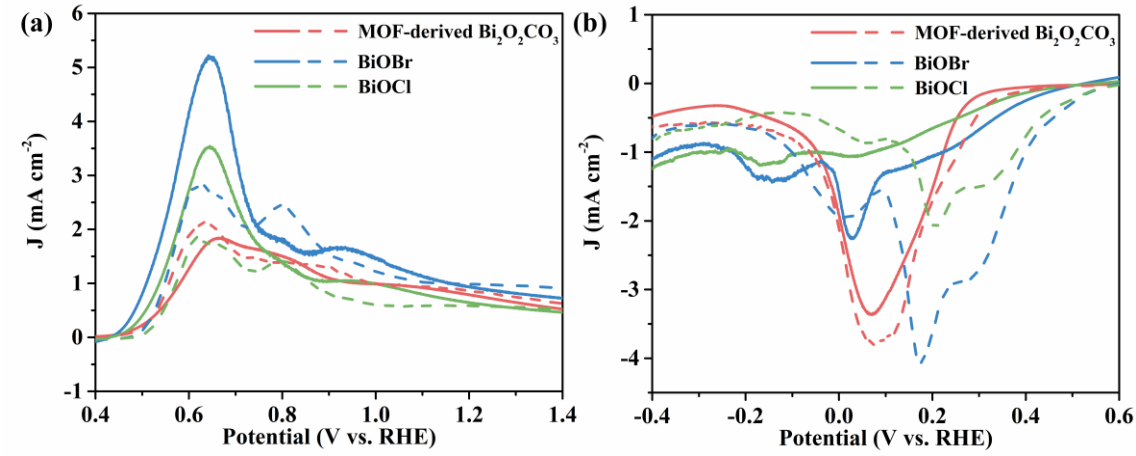

Fig. S16 Partial enlarged (a) oxidation curves and (b) reduction curves drawings of Fig. 5a. The solid and dotted line separately reacted in CO_2- and N_2-saturated 0.5 M $KHCO_3$ electrolyte.

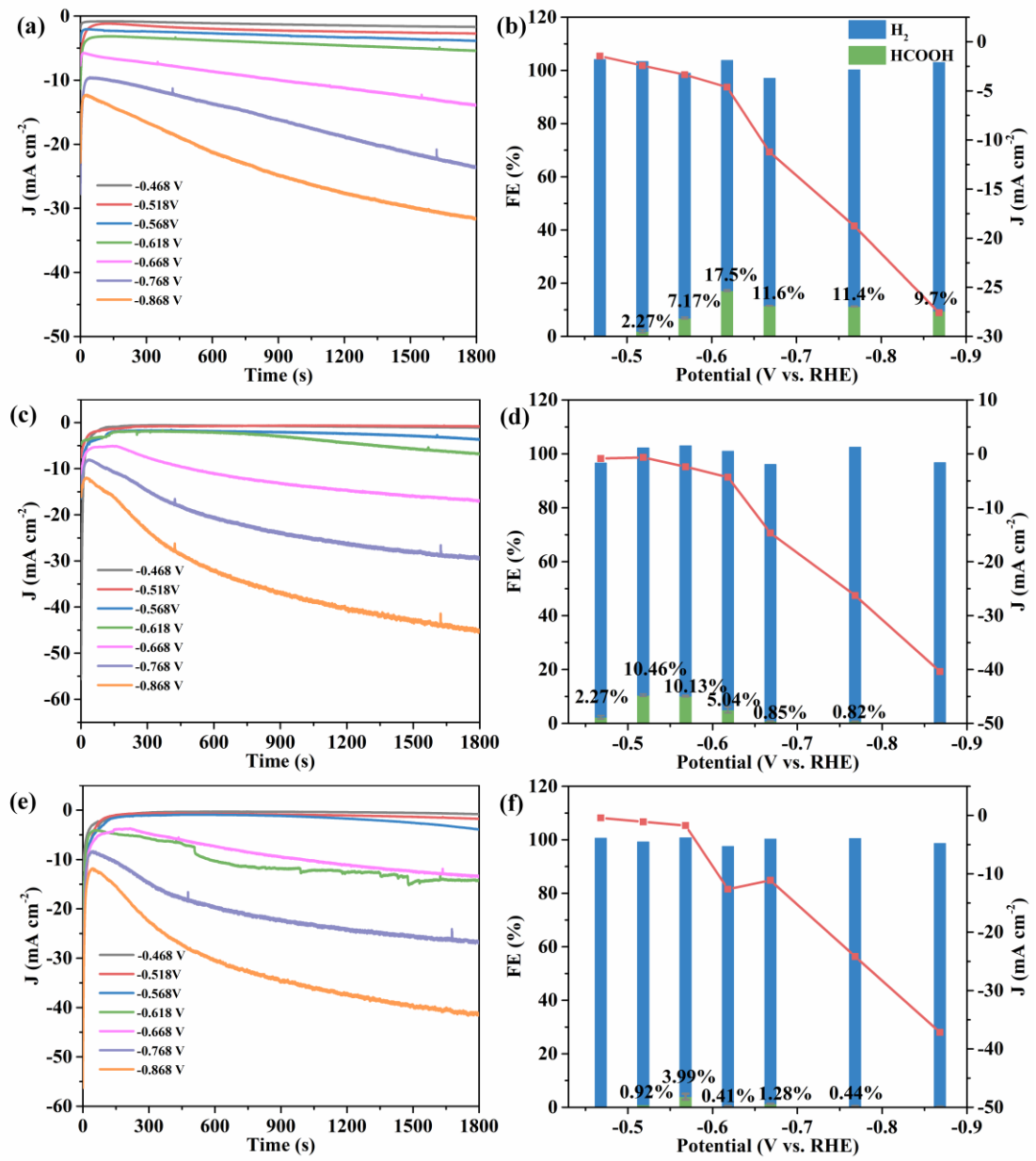

Fig. S17 Total current densities of (a) MOF-derived $Bi_2O_2CO_3$, (c) BiOBr and (e) BiOCl in 15% CO_2 + 85% N_2 0.5 M $KHCO_3$ electrolyte at different potentials from -0.468 V to -0.868V vs. RHE as indicated. Faradaic efficiencies of products for (b) MOF-derived $Bi_2O_2CO_3$, (d) BiOBr and (f) BiOCl at each applied potential.

The gas mixture with 15% CO_2 and 85% N_2 is controlled by the flow rate of the two gases. Selected 1.5 sccm CO_2 and 8.5 sccm N_2 to ensure the total flow rate is 10 sccm. The electrolyte is N_2-saturated (pH = 9.14) before the mixture gases blowing. p

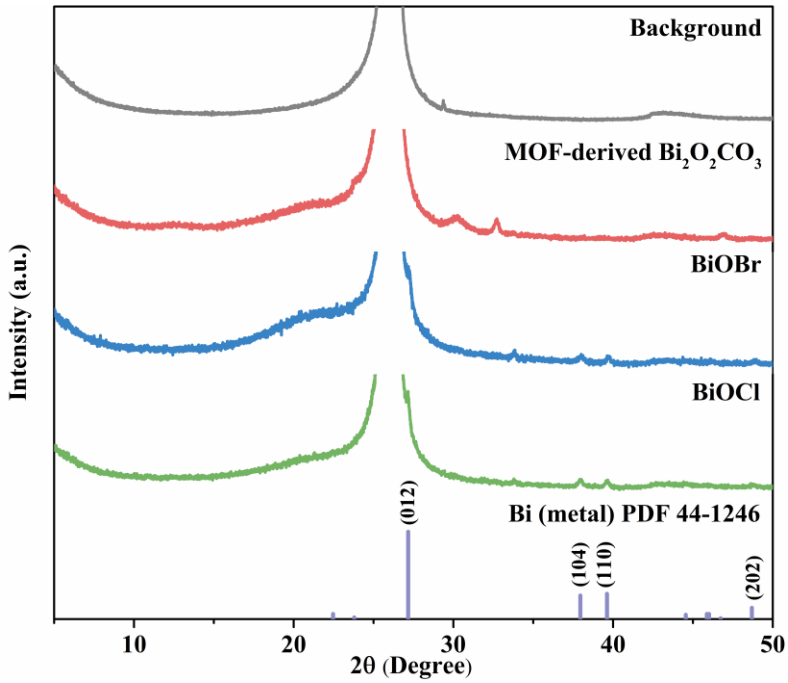

Fig. S18 XRD patterns of MOF-derived $Bi_2O_2CO_3$/carbon paper electrode (firebrick), BiOBr/carbon paper electrode (steelblue) and BiOCl/carbon paper electrode (green) after 0.5 h electrolysis at -0.669 V vs. RHE. The background is carbon paper electrode (grey). It is noted that this XRD pattern of carbon paper electrode has no peak at 18.16° compared with the Fig.3a because of using different carbon papers.

Table S1 Summary and comparison of the catalytic performance with other electrocatalysts materials for eCO_2RR to formate.

Catalyst	Electrolyte	Potential	FE_{HCOO^-}	Stability	Ref.
MOF-derived $Bi_2O_2CO_3$	0.5 M $KHCO_3$	-0.669 V vs. RHE	96.1%	48 h (over 93%)	This work
Bi_2O_3NSs@ MCCM	0.1 M $KHCO_3$	-1.265 V vs. RHE	93.8%	12 h at -0.956 V vs. RHE (around 76.3%)	3
AgBi-500	0.1 M $KHCO_3$	-0.7 V vs. RHE	94.3%	12 h (over 90%)	5
Bi-based NPs	0.5 M $KHCO_3$	-0.97 V vs. RHE	95%	32 h (over 80%)	6
Bi NSs	0.5 M $KHCO_3$	-0.826 V vs. RHE	~100%	10 h (around 95%)	7
Bi nanostructure	0.5 M $KHCO_3$	-0.9 V vs. RHE	92%	10 h (over 82.35%)	8
Bi nanoflakes	0.1 M $KHCO_3$	-0.8 V vs. RHE	90%	10 h (over 90%)	9
$[Fe_4N(CO)_{12}]^-$	0.1 M phosphate (pH=7)	-0.55 vs. RHE	95%	24 h (over 90%)	10
In_2O_3-rGO	0.1 M $KHCO_3$	-1.2 V vs. RHE	90%	10 h (over 80%)	11
In-BDC	0.5 M $KHCO_3$	-0.669 V vs. RHE	88%	21 h (over 70%)	12
Sn dendrite	0.1 M $KHCO_3$	-1.36 V vs. RHE	83.4%	18 h (over 71.6%)	13

Table S2 Summary and comparison of the TOF with other electrocatalysts for eCO_2RR.

Catalyst	Electrolyte	Products	Potential	TOF	Ref.
MOF-derived $Bi_2O_2CO_3$	0.5 M $KHCO_3$	Formate	-0.969 V vs. RHE	2207 h^{-1}	This work
$[Fe_4N(CO)_{12}]^-$	0.1 M phosphate (pH=7)	Formate	-1.2 V vs. SCE	106±6 h^{-1}	10
In-BDC	0.5 M $KHCO_3$	Formate	-1.069 V vs. RHE	4789 h^{-1}	12
Cu_2(CuTCPP)	0.5 M $KHCO_3$	Formate	-1.55 V vs. Ag/Ag^+	2037 h^{-1}	14
Cu-CB/GDL	0.5 M KCl	All products including formate	-1.1 V vs. RHE	72 h^{-1}	15
Co protoporphyrin	1 mM $HClO_4$ + 99 mM $NaClO_4$	CO	-0.8V vs. RHE	2880 h^{-1}	16
MOF-525	1 M $TBAPF_6$ in ACN	CO	-0.65 V vs. RHE	64 h^{-1}	17
2D $Ni(Im)_2$-5 nm	0.5 M $KHCO_3$	CO	-0.95 V vs. RHE	770 h^{-1}	18
CoTPP	0.5 M $KHCO_3$	CO	-1.35 V vs. SCE	288 h^{-1}	19
CuO/SnO_2	0.1 M $NaHCO_3$	CO	-0.9 V vs. RHE	886 h^{-1}	20
$Al_2(OH)_2$TCPP-Co	0.5 M $KHCO_3$	CO	-0.7 V vs. RHE	200 h^{-1}	21

Reference

1 E. Zhang, T. Wang, K. Yu, J. Liu, W. Chen, A. Li, H. Rong, R. Lin, S. Ji, X. Zheng, Y. Wang, L. Zheng, C. Chen, D. Wang, J. Zhang and Y. Li, *J. Am. Chem. Soc.*, 2019, **141**, 16569-16573.

2 N. Han, Y. Wang, L. Ma, J. Wen, J. Li, H. Zheng, K. Nie, X. Wang, F. Zhao, Y. Li, J. Fan, J. Zhong, T. Wu, D. J. Miller, J. Lu, S. T. Lee and Y. Li, *Chem*, 2017, **3**, 652-664.

3 S. Liu, X. F. Lu, J. Xiao, X. Wang and X. W. Lou, *Angew. Chem., Int. Ed.*, 2019, **58**, 13828-13833.

4 F. Yang, X. Ma, W. B. Cai, P. Song and W. Xu, *J. Am. Chem. Soc.*, 2019, **141**, 20451-20459.

5 J. H. Zhou, K. Yuan, L. Zhou, Y. Guo, M. Y. Luo, X. Y. Guo, Q. Y. Meng and Y. W. Zhang, *Angew. Chem., Int. Ed.*, 2019, **58**, 14197-14201.

6 P. Lamagni, M. Miola, J. Catalano, M. S. Hvid, M. A. H. Mamakhel, M. Christensen, M. R. Madsen, H. S. Jeppesen, X. M. Hu, K. Daasbjerg, T. Skrydstrup and N. Lock, *Adv. Funct. Mater.*, 2020, **30**, 1910408.

7 N. Han, Y. Wang, H. Yang, J. Deng, J. Wu, Y. Li and Y. Li, *Nat. Commun.*, 2018, **9**, 1320.

8 P. Lu, D. Gao, H. He, Q. Wang, Z. Liu, S. Dipazir, M. Yuan, W. Zu and G. Zhang, *Nanoscale*, 2019, **11**, 7805-7812.

9 S. Kim, W. J. Dong, S. Gim, W. Sohn, J. Y. Park, C. J. Yoo, H. W. Jang and J. L. Lee, *Nano Energy*, 2017, **39**, 44-52.

10 A. Taheri, E. J. Thompson, J. C. Fettinger and L. A. Berben, *ACS Catal.*, 2015, **5**, 7140-7151.

11 Z. Zhang, F. Ahmad, W. Zhao, W. Yan, W. Zhang, H. Huang, C. Ma and J. Zeng, *Nano Lett.*, 2019, **19**, 4029-4034.

12 S. Z. Hou, X. D. Zhang, W. W. Yuan, Y. X. Li and Z. Y. Gu, *Inorg. Chem.*, 2020, **59**, 11298-11304.

13 D. H. Won, C. H. Choi, J. Chung, M. W. Chung, E. H. Kim and S. I. Woo, *ChemSusChem*, 2015, **8**, 3092-3098.

14 J. X. Wu, S. Z. Hou, X. D. Zhang, M. Xu, H. F. Yang, P. S. Cao and Z. Y. Gu, *Chem. Sci.*, 2019, **10**, 2199-2205.

15 C. Ampelli, C. Genovese, B. C. Marepally, G. Papanikolaou, S. Perathoner and G. Centi, *Faraday. Discuss.*, 2015, **183**, 125-145.

16 J. Shen, R. Kortlever, R. Kas, Y. Y. Birdja, O. D. Morales, Y. Kwon, I. L. Yanez, K. J. P. Schouten, G. Mul and M. T. M. Koper, *Nat. Commun.*, 2015, **6**, 8177.

17 I. Hod, M. D. Sampson, P. Deria, C. P. Kubiak, O. K. Farha and J. T. Hupp, *ACS Catal.*, 2015, **5**, 6302-6309.

18 J. X. Wu, W. W. Yuan, M. Xu and Z. Y. Gu, *Chem. Commun.*, 2019, **55**, 11634-11637.

19 X. M. Hu, M. H. Rønne, S. U. Pedersen, T. Skrydstrup and K. Daasbjerg, *Angew. Chem., Int. Ed.*, 2017, **56**, 6468-6472.

20 M. Schreier, F. Héroguel, L. Steier, S. Ahmad, J. S. Luterbacher, M. T. Mayer, J. Luo and M. Grätzel, *Nat. Energy*, 2017, **2**, 17087.

21 N. Kornienko, Y. Zhao, C. S. Kley, C. Zhu, D. Kim, S. Lin, C. J. Chang, O. M. Yaghi and P. Yang, *J. Am. Chem. Soc.*, 2015, **137**, 14129-14135.